Processing and Application of Ceramics 19 [4] (2025) 352–358
https://doi.org/10.2298/PAC2504352A

Stoichiometric nepheline ($NaAlSiO_4$) glass: Synthesis, crystallization and characterization with relevance to dentistry

Ali S. Alzahrani*

Department of Oral Medicine and Allied Dental Sciences, College of Dentistry, Taif University, P.O. Box 11099, Taif, 21944, Saudi Arabia

Received 25 August 2025; Received in revised form 11 November 2025; Accepted 30 November 2025

Abstract

Stoichiometric nepheline ($NaAlSiO_4$) glass was synthesized via the melt-quenching technique at 1650 °C for 3 h and prepared in two different forms: i) bulk glass, obtained by casting the melt into a graphite mould and post annealing in a preheated furnace at 450 °C and ii) glass frit, obtained by quenching the crucible containing the remaining melt in water and subsequent compacting. The obtained glass samples were subjected to controlled crystallization at 1000 °C for 24 h. The thermal, structural and microstructural characteristics were investigated using differential scanning calorimetry (DSC), X-ray diffraction (XRD), dilatometry, ^{23}Na and ^{27}Al MAS-NMR spectroscopy and scanning electron microscopy (SEM). The results confirmed the formation of nepheline as the primary crystalline phase, with directional dendritic and prismatic morphologies evident after heat treatment. Crystallization was dominated by surface nucleation mechanisms and an increase in glass particle size of the frit was found to elevate the crystallization temperature. These findings provide fundamental insights into the crystallization pathways of nepheline glass and establish its potential relevance in future dental applications.

Keywords: *nepheline glass, crystallization kinetics, Avrami analysis, surface nucleation, dental application*

I. Introduction

Multi-component nepheline-based glass and glass-ceramic systems are widely used in industrial applications, including ceramics, coatings and structural materials, due to their favourable thermal stability and chemical durability. Recently, attention has shifted toward exploring their potential in biomedical fields, particularly in dental and medical applications, where the demand for durable glass-ceramic materials is growing.

Nepheline is a sodium aluminosilicate ($NaAlSiO_4$) structurally derived from the silicate polymorph tridymite [1]. It commonly occurs in silica-deficient feldspathoid minerals and often incorporates minor amounts of potassium, forming compositions such as $(Na,K)AlSiO_4$ [2]. Substitution of sodium by potassium or calcium within the silicate framework has been reported, influencing both structural stability and phase development [3,4]. Previous studies have partially examined the solid-solution behaviour of nepheline, with particular emphasis on the effect of the Na:K ratio [5]. Increasing potassium content can promote the crystallization of kalsilite ($KAlSiO_4$), while variations in the Si:Al ratio may favour the formation of leucite ($KAlSi_2O_6$), albite ($NaAlSi_3O_8$), or mixed feldspar-type phases [6–8]. These compositional variations highlight the sensitivity of nepheline-based systems to subtle chemical modifications, which in turn govern the crystalline phases and microstructures that develop during processing.

Glass-ceramics containing nepheline in their structure have attracted considerable attention due to their ion-exchange capability ($Na^+ \leftrightarrow K^+$), which can significantly enhance their mechanical properties. For example, ion-exchanged nepheline-based glass-ceramics have been reported to exhibit flexural strength increases from <200 MPa up to 2200 MPa [9]. Additionally, nepheline-based glass-ceramics exhibit excellent chemical, abrasion and stain resistance, low thermal expansion, low porosity and favourable aesthetic appearance, making them highly suitable for dental applications [10–14]. Naturally occurring nepheline has

*Corresponding author: +966127342675
e-mail: *asalzahrani@tu.edu.sa*

a Mohs hardness of 5.5–6.0, comparable to human enamel [5,15], and refractive indices ranging from 1.52 to 1.54, closely matching those of enamel (1.63) and dentine (1.54) [16]. Nepheline's transparency to translucency, with yellowish-white or colourless appearance, further enhances its potential in aesthetic dental restorations [17,18].

Although numerous studies have investigated complex nepheline-containing compositions, relatively little emphasis has been placed on stoichiometric nepheline ($NaAlSiO_4$) glass as a model system. Understanding its crystallization behaviour and microstructural development is critical to evaluating its suitability for biomedical adaptation, since the performance of dental glass-ceramics is closely linked to their crystalline phases and microstructural characteristics.

The objective of this study is to synthesize, crystallize and characterize stoichiometric nepheline glass using highly pure reagents. By employing a comprehensive suite of characterization techniques, including DSC, XRD, dilatometry, MAS-NMR and SEM, this work aims to provide a detailed account of the structural evolution and crystallization mechanisms in nepheline glass. The insights gained will contribute to establishing fundamental structure-property relationships, thereby informing the potential translation of nepheline-based glass systems into dental materials research.

II. Experimental

2.1. Glass synthesis

A glass with a chemical composition of 25 Na_2O-25 Al_2O_3-50 SiO_2 (mol%), representing the stoichiometric composition of nepheline, was synthesised using the melt-quench technique. The homogeneous mixture containing high purity grades of silica (SiO_2, 98%), aluminium oxide (Al_2O_3, 99.9%) and sodium carbonate (Na_2CO_3, 99%) was prepared. The batch, corresponding to 100 g of oxide glass, was melted in Pt-Rh crucible in an electric furnace at 1650 °C for 3 h. The glass was prepared in two different forms, namely bulk and frit. The bulk glass was obtained by casting the melt into a graphite mould measuring approximately $6 \times 6 \times 25$ mm for dilatometry analysis. The cast was then annealed in a preheated furnace at 450 °C for 2 h. On the other hand, the glass frit was obtained by quenching the crucible containing the remaining melt in water. The resulting glass frit was then dried, dry ball milled using alumina milling media and compressed. Different meshs were used and three frit samples, NAS <45, NAS 45–125 and NAS >125, were prepared with different particle sizes, i.e. <45, 45–125 and >125 μm, respectively.

2.2. Crystallization of the prepared glass

Two forms of the same glass, bulk and dry compressed frit, were selected for heating: i) the bulk glass fragments cut from the annealed glass and ii) green body specimens made from glass frit with particle sizes 45–125 μm. The dry compression was done under a pressure of 1 bar for a period of 1 min. Both compressed frit and bulk glass were subjected to simultaneous thermal treatment in the same furnace at 1000 °C for 24 h in air, with a heating rate of 20 °C/min, starting and ending at room temperature. The crystallized samples obtained from the glass frit were used for X-ray diffraction and nuclear magnetic resonance experiments.

2.3. Differential scanning calorimetry

Crystalline phase evolution in the glass has been investigated under non-isothermal conditions using differential scanning calorimetry (DSC 204F1-Netzch), with a temperature range from 25 °C to a maximum of 1200 °C, at a heating rate of 20 °C/min. Aluminium oxide (Al_2O_3) has been used as a reference material and a sample of 50 mg (±0.5) has been measured in a platinum crucible. The experiment was carried out in a flowing nitrogen atmosphere set at 60 ml/min. In order to understand the effect of surface area on heat flow, the study investigated the crystallisation mechanism of glasses obtained by using the frits with different particle sizes (<45 μm, 45–125 μm and >125 μm) at a fixed heating rate of 20 °C/min. The calorimetric glass transition temperature T_g, the maximum crystallisation temperature T_c and the endothermic T_m were obtained from the DSC experiments.

Avrami analysis from DSC data

The crystallization kinetics of the synthesized nepheline glass was evaluated using non-isothermal differential scanning calorimetry (DSC) at a constant heating rate of 20 °C/min. The glass samples, obtained by using the frits with different particle sizes (<45, 45–125 and >125 μm), were analysed to investigate the effect of particle size on nucleation and growth mechanisms.

The relative crystallized fraction (X) at any temperature T was calculated from the DSC exotherm using:

$$X(T) = \frac{\int_{T_0}^{T} \left(\frac{dH}{dT}\right) dT}{\int_{T_0}^{T_f} \left(\frac{dH}{dT}\right) dT} \tag{1}$$

where T_0 is onset crystallization temperature, T_f is final crystallization temperature and dH/dT is DSC heat flow. The Johnson-Mehl-Avrami-Kolmogorov (JMAK) model was applied to describe the crystallization kinetics:

$$X(t) = 1 - \exp(-K \cdot t^n) \tag{2}$$

where $X(t)$ is fraction crystallized at time t, K is overall crystallization rate constant and n is Avrami exponent, describing the nucleation and growth mechanism. For non-isothermal conditions at constant heating rate (β):

$$t = \frac{T - T_0}{\beta} \tag{3}$$

the equation can be linearized as:

$$\ln[-\ln(1-X)] = n \cdot \ln(t) + \ln(K) \quad (4)$$

By plotting $\ln[-\ln(1-X)]$ versus $\ln(t)$, the slope of the fitted line yields the Avrami exponent (n), and the intercept provides $\ln(K)$.

The Avrami exponent (n) provides insight into the crystallization mechanism: $n \approx 1$ indicates one-dimensional crystal growth with instantaneous nucleation; $n \approx 2$ corresponds to two-dimensional growth or sporadic nucleation; $n \approx 3$ suggests three-dimensional bulk growth with uniform nucleation and $n > 3$ implies three-dimensional growth accompanied by an increasing nucleation rate [19].

2.4. Structural characterization

Dilatometric analysis was carried out using a differential dilatometer (DIL, 402PC, Netzsch, Germany) on a rectangular glass rod measuring about 6 × 6 × 25 mm (±0.5 mm). The glass sample was heated in a flowing nitrogen atmosphere (1 ml/min) at a heating rate of 3 °C/min from 25 to 1200 °C. The glass transition temperature (T_g), dilatometric softening point and coefficient of thermal expansion (CTE) were determined using thermal analysis software (NETZSCH Proteus 402 PC). The CTE data were extracted in the range of 100 to 500 °C.

X-ray diffraction was carried out on the glass before and after the heat treatment using an X-ray diffractometer (Panalytical X'Pert Pro, Netherlands), with Cu-Kα radiation at wavelengths of 1.5405980 Å and 1.5444260 Å, operating at 45 kV and 40 mA. X-ray diffraction data were collected in $2\theta = 5°$ to 70° range with a step size of 0.0334° and a step time equivalent to 200 s/°. The collected data were analysed using Match! Fullprof software.

The heat treated bulk glass samples were mounted in epoxy resin, polished to a mirror finish and then etched in 0.5 vol.% hydrofluoric acid for 0.5 min to partially remove the glassy phase and improve image contrast. The etched surface was then gold coated and viewed using a field emission scanning electron microscope (JSM 6300F, JEOL Ltd, SEM, UK).

^{23}Na and ^{27}Al MAS-NMR spectra were collected on the glass before and after heat treatment, using a Bruker 600 MHz (14.1 T) nuclear magnetic resonance spectrometer. A single resonance Bruker probe was used in a 4 mm rotor. A resonance frequency of 159, 156 MHz, a single pulse duration of 1 µs and a recycle delay time of 1 s were used for ^{23}Na and ^{27}Al, respectively, at a spin rate of 12 kHz. The isotopic chemical shifts for each nucleus were referenced to 0 ppm using signals acquired from the standard reference solutions, sodium chloride (NaCl) and aluminium nitrate $Al(NO_3)_3$, respectively. TopSpin 4.0.5 software was used to analyse the collected data.

III. Results and discussion

3.1. Thermal behaviour

DSC analysis of the NAS 45–125 glass (Fig. 1) showed typical glass behaviour, with clearly visible glass transition temperature (T_g), exothermic crystallization peak (T_c) and endothermic event. It can be seen (Fig. 1) that the crystallization temperature of the obtained glasses increases with particle size of the frit, and is 973 °C, 1027 °C and 1095 °C for the samples NAS <45, NAS 45–125 and NAS >125, respectively (Table 1). This indicates surface-dominated nucleation. The reduced glass transition temperature, ($T_{rg} \approx 0.67$) confirms that surface crystallization is the primary devitrification mechanism, consistent with literature for glasses lacking internal nucleating agents [19,20].

Dilatometry of the bulk glass sample (Fig. 2) revealed that glass transition temperature is T_g = 783 °C and softening temperature is 877 °C (Table 1). The coefficient of linear thermal expansion between 100–500 °C is 10.47×10^{-6} K^{-1}, indicating low thermal expansion - a key property for dental restoratives to minimize thermal mismatch. The synthesized stoichiomet-

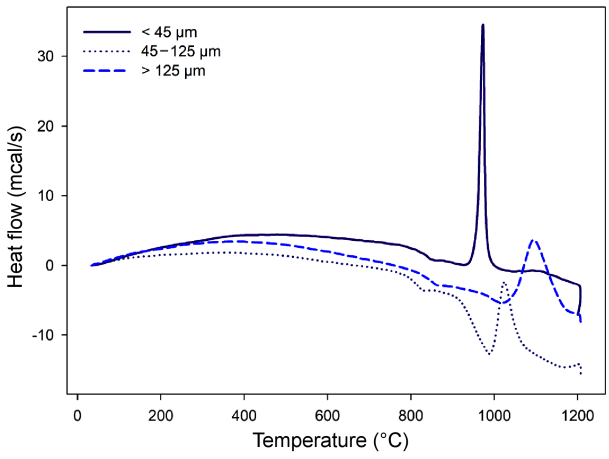

Figure 1. DSC traces obtained at heating rate of 20 °C/min of three glassy $NaAlSiO_4$, prepared with frits with three different glass particle sizes <45, 45–125 and >125 µm showing the effect of surface area on the heat flow

Table 1. Extracted data from DSC and dilatometer: glass transition temperatures (T_g), softening temperatures (T_s), maximum peak for crystallization (T_c), melting temperature (T_m) and coefficient of thermal expansion (CTE)

Sample	Particle size	T_g [°C] DSC	T_g [°C] dilatometer	T_s [°C] dilatometer	T_c [°C] DSC	T_m [°C] DSC	CTE [K^{-1}] (100–500 °C)
NAS <45	<45 µm	810			973	1207	
NAS 45–125	45–125 µm	798			1027	1204	
NAS >125	>125 µm	806	783	877	1095	1207	10.47×10^{-6}

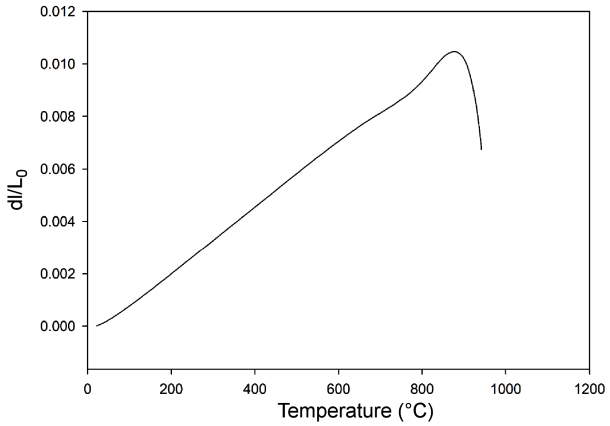

Figure 2. Dilatometry curve of the stoichiometric $NaAlSiO_4$ glass (sample NAS >125)

ric nepheline glass is transparent and amorphous as confirmed by XRD (Fig. 3a), whereas after heating at 1000 °C it transforms into pure tetragonal nepheline phase (Fig. 3b).

3.2. Crystallization kinetics (Avrami analysis)

The crystallization behaviour of stoichiometric nepheline glass was analysed using DSC at a constant heating rate of 20 °C/min for the glass prepared from three particle size fractions (<45, 45–125 and >125 μm). The relative crystallized fraction (X) was derived from DSC exotherms, and the Avrami model was applied to evaluate the nucleation and growth mechanisms. Figure 4 shows the Avrami plots of $\ln[-\ln(1-X)]$ versus $\ln(t)$ for the samples NAS <45, NAS 45–125 and NAS >125. The slopes represent the Avrami exponents (n), revealing the crystallization mechanisms influenced by particle size.

The calculated Avrami exponents (n) are all greater than 4 (Table 2), indicating that crystallization proceeds through a three-dimensional growth mechanism with an increasing nucleation rate. The samples NAS <45 and NAS 45–125, prepared by frit with smaller particle sizes, exhibit slightly lower n values compared to the sample NAS >125 obtained by using frit with coarser fraction. This indicates that finer glass particles nucleate earlier, while larger particles enhance surface-driven crystallization due to a lower surface-to-volume ratio.

These findings are consistent with SEM observations showing dendritic and prismatic crystal morphologies growing from the surface into the bulk. The interlocked crystal structure contributes to the mechanical reinforcement by limiting microcrack propagation, which is highly desirable for dental glass-ceramic applications.

By controlling particle size and crystallization conditions, the final microstructure can be tailored to achieve specific performance targets. This optimization is crucial for dental restorative applications where high strength, thermal compatibility and aesthetic properties are required. The ability to obtain a homogeneous nepheline crystalline phase with predictable nucleation pathways supports its potential as a high-performance dental glass-ceramic material.

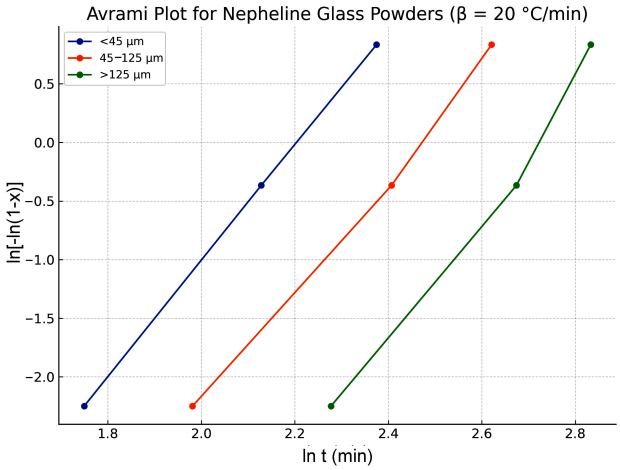

Figure 4. Dilatometry curve of the stoichiometric $NaAlSiO_4$ glass (sample NAS >125)

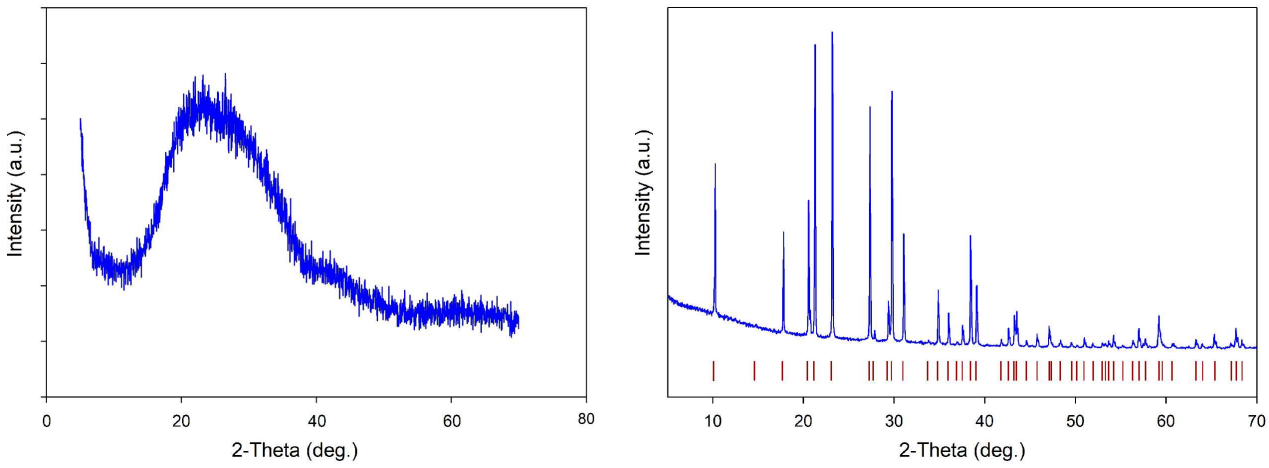

Figure 3. XRD patterns for stoichiometric $NaAlSiO_4$ glass before (a) and after heating at 1000 °C for 24 h (b) showing amorphous glass and only nepheline crystalline phase after 24 h crystallizations

Table 2. Avrami exponents (n) of glasses obtained by using frits with different particle sizes

Sample	Particle size	Avrami exponent, n	Crystallization mechanism
NAS <45	<45 μm	4.93	3D growth with increasing nucleation rate
NAS 45–125	45–125 μm	4.76	3D growth with increasing nucleation rate
NAS >125	>125 μm	5.39	Accelerated 3D surface-driven growth

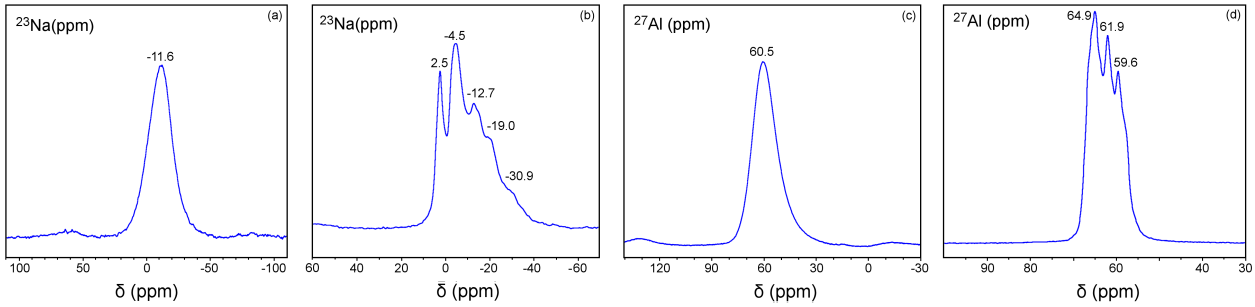

Figure 5. ^{23}Na and ^{27}Al MAS-NMR spectra of NAS 45–125 glass before (a,c) and after (b,d) crystallization at 1000 °C for 24 h

3.3. MAS-NMR analysis

Figure 5 present the ^{23}Na and ^{27}Al MAS-NMR spectra of the as-prepared glass displayed broad peaks at −11.6 ppm (^{23}Na) and 60.5 ppm (^{27}Al), characteristic of amorphous aluminosilicates with Na^+ as charge-compensating cation and Al predominantly in tetrahedral coordination. After crystallization at 1000 °C for 24 h, ^{23}Na peaks shifted to −4.5 ppm, indicating a more uniform arrangement of sodium in the crystalline nepheline phase. ^{27}Al spectra exhibited peaks at 59.6, 61.9 and 64.9 ppm, corresponding to tetrahedrally coordinated aluminium in residual glass and nepheline. These structural transformations support the formation of a dominant crystalline phase while retaining a minor amorphous fraction, crucial for balancing aesthetics and mechanical strength in dental glass-ceramics.

The MAS-NMR data probe two quadrupolar nuclei that are highly diagnostic for aluminosilicates: ^{27}Al (I = 5/2) and ^{23}Na (I = 3/2). In the as-prepared glass, the ^{27}Al peak at 60.5 ppm indicates tetrahedral Al[4] coordination, while the ^{23}Na resonance at −11.6 ppm reflects sodium acting as a charge-compensating cation within a disordered network. After crystallization, multiple ^{27}Al peaks at 59.6, 61.9 and 64.9 ppm arise from distinct Al[4] sites in nepheline and residual glass fractions. The ^{23}Na spectra shift to a dominant −4.5 ppm peak, evidencing sodium incorporation into ordered framework cavities of nepheline, while residual amorphous environments persist, as indicated by broad negative shoulders and a minor positive-shift feature near 2.5 ppm.

These spectral changes reflect structural ordering during nepheline crystallization, with Na redistribution from charge-compensating glassy sites into well-defined crystalline positions. Persistent residual glass accounts for a fraction of unstructured Na environments. The results are consistent with XRD patterns and SEM observations showing dendritic and prismatic nepheline growth interspersed with residual amorphous pockets. This structural insight also supports potential ion exchangeability of Na in near-surface regions, relevant for strengthening treatments in dental applications.

3.4. Microstructure

SEM analysis of the crystallized bulk glass revealed well-defined dendritic and prismatic nepheline crystals extending from the surface into the bulk (Fig. 6). Thus, the crystals exhibit core-shell type morphology, where the “core” represents the early-formed, densely packed nepheline nucleus with a highly ordered aluminosilicate structure. The “shell” consists of later-grown dendritic regions formed under diffusion-controlled conditions, leading to more open and branching microstructures. This zoning reflects compositional gradients during crystal growth. The observed interlocked crystal structure enhances mechanical integrity and minimizes microcrack propagation.

Surface cracks at the glass-crystal interface were attributed to localized thermal stresses during crystallization, but the crystalline interior remained crack-free (Fig. 6). The inner region of the crystal that forms first during nucleation acts as the starting point from which the rest of the crystal grows. Crystal morphologies and growth mechanisms are consistent with dendritic, prismatic and hexagonal habits reported in mineralogical studies [32,33], providing microstructural reinforcement desirable for load-bearing dental restorations.

3.5. Dental relevance

The synthesized nepheline glass-ceramics exhibits thermal stability, low thermal expansion, interlocked crystal microstructure and controlled surface nucleation, all of which are highly advantageous for dental applications. Its Mohs hardness and optical properties closely match those of enamel and dentine, supporting wear resistance and aesthetic integration. Additionally, the ion-exchange capability ($Na^+ \leftrightarrow K^+$) offers potential for surface strengthening treatments, enhancing durability in restorative systems such as crowns, bridges, and veneers. Overall, the combination of structural, thermal

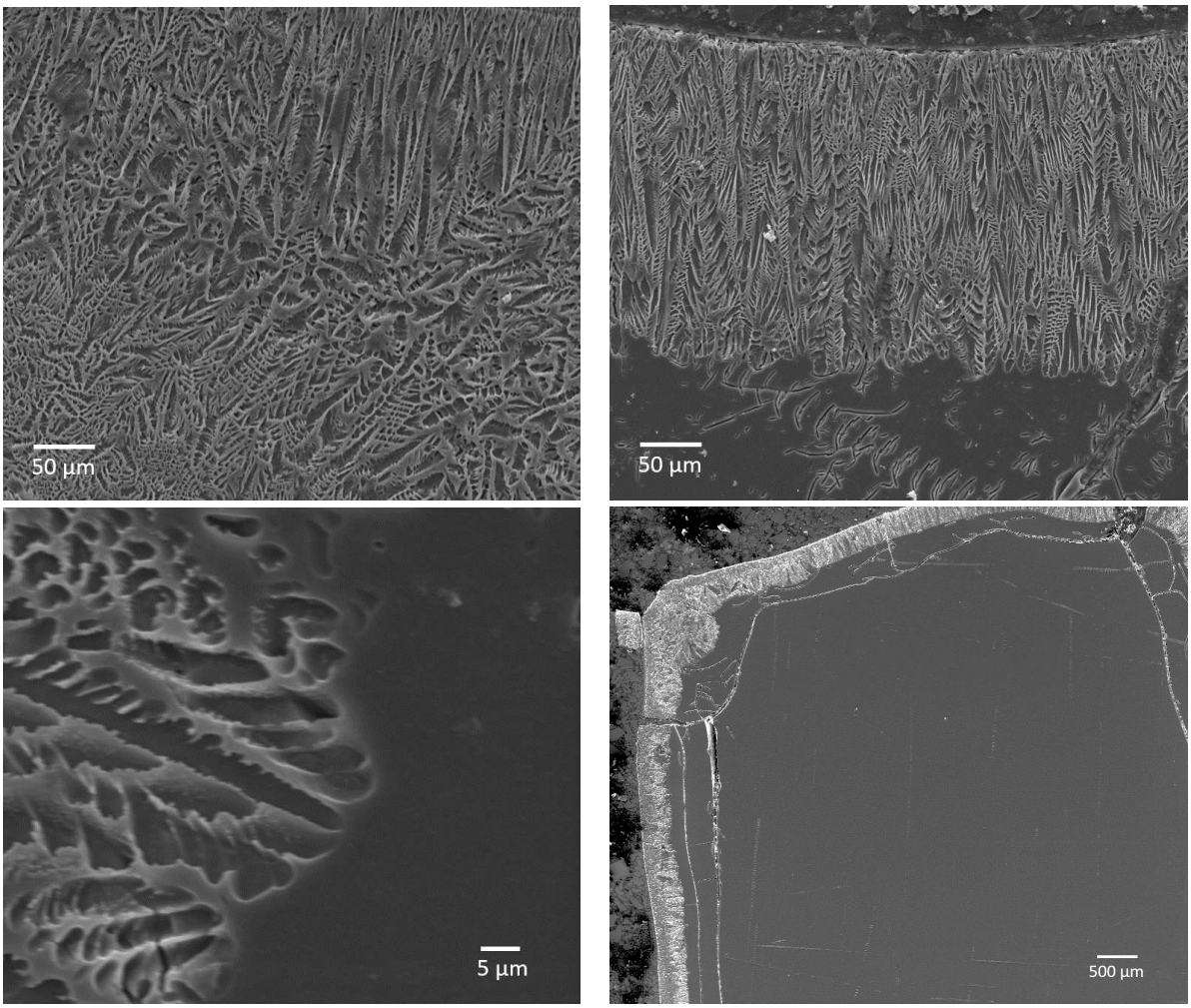

Figure 6. SEM micrographs at different magnifications of stoichiometric $NaAlSiO_4$ bulk glass heat treated at 1000 °C for 24 h

and microstructural properties positions stoichiometric nepheline glass as a promising candidate for future dental glass-ceramic research [11].

The coefficient of thermal expansion (CTE) of the synthesized nepheline glass, measured between 100 and 500 °C, was found to be $10.47 \times 10^{-6}\,K^{-1}$. This value falls within the range commonly reported for dental ceramics and glass-ceramics (~8–13 $\times$ $10^{-6}\,K^{-1}$) [12]. Such compatibility is crucial as a CTE mismatch between the restorative material and veneering porcelains (~9–12 $\times$ $10^{-6}\,K^{-1}$) can lead to microcracking, interfacial debonding, or catastrophic failure. The CTE value of nepheline glass synthesized in this study therefore indicates promising potential for dental applications, particularly as a candidate glass-ceramic framework or as a reinforcing phase in composite dental materials.

IV. Conclusions

Stoichiometric nepheline ($NaAlSiO_4$) glass was successfully synthesized via the melt-quenching method and crystallized through controlled heat treatment at 1000 °C for 24 h. Thermal analysis confirmed high glass transition and crystallization temperatures, with surface nucleation as the dominant devitrification mechanism. MAS-NMR and XRD analyses demonstrated the formation of a single-phase nepheline crystalline structure while retaining a minor residual amorphous fraction, and SEM revealed well-defined dendritic and prismatic interlocked crystal morphologies.

The synthesized nepheline glass-ceramics exhibits a combination of favourable properties - including low thermal expansion, high thermal stability, mechanical robustness and structural homogeneity - that are directly relevant to dental applications. Its hardness, optical transparency and refractive index closely match those of natural enamel and dentine, supporting both wear resistance and aesthetic integration. Furthermore, the potential for ion-exchange surface strengthening enhances its suitability for durable dental restoratives such as crowns, bridges and veneers.

Overall, this study provides fundamental insights into the structure-property relationships of stoichiometric nepheline glass, establishing a foundation for future research and development of nepheline-based glass-ceramic materials for advanced dental applications.

Acknowledgement: The author would like to acknowledge the Deanship of Graduate Studies and Scientific Research, Taif University for funding this work.

References

1. C.J. Koenig, "Use of nepheline syenite in sanitary porcelain", *J. Am. Ceram. Soc*., **22** (1939) 38–46.
2. P. Saha, "The system $NaAlSiO_4$ (nepheline)-$NaAlSi_3O_8$ (albite)-H_2O", *Am. Mineral*., 46 [7-8] (1961) 859–884.
3. H.G. Winkler, "On the synthesis of nepheline", *Am. Mineral*., **32** [3-4] (1947) 131–136.
4. F.A. Bannister, M.H. Hey, "A chemical, optical, and X-ray study of nepheline and kaliophilite", *Mineral. Magaz*., **22** (1931) 569–608.
5. G. Rossi, R. Oberti, D.C. Smith, "The crystal structure of a K-poor Ca-rich silicate with the nepheline framework", *Eur. J. Mineral*., **1** (1989) 59–70.
6. J.V. Smith, T.G. Sahama, "Determination of the composition of natural nephelines by an X-ray method", *Mineral. Magaz*., **30** (1954) 439–449.
7. J.V. Smith, O.F. Tuttle, "The nepheline-kalsilite system; Part I, X-ray data *Chem. Geology* for the crystalline phases", *Am. J. Sci*., **255** [4] (1957) 282–305.
8. J.M. Ferry, J.G. Blencoe, "Subsolidus phase relations in the nepheline-kalsilite system", *Am. Mineral*., **63** [11-12] (1978) 1225–1240.
9. D.A. Duke, J.F. MacDowell, B.R. Karstetter, "Crystallization and chemical strengthening of nepheline glass-ceramics", *J. Am. Ceram. Soc*., **50** [2] (1967) 67–74.
10. A.S. Alzahrani, "Syntheses and characterization of twofold nepheline-combeite glass-ceramics for dental application", *J. Non-Crystal. Solids*, **596** (2022) 121877.
11. A.S. Alzahrani, "Novel ion-exchangeable nepheline glass-ceramics for dental application", *J. Eur. Ceram. Soc*., **43** [13] (2023) 5682–5690.
12. A.S. Alzahrani, "Effect of TiO_2 on the sinter crystallization of nepheline glasses for dental application", *Int. J. Appl. Glass Sci*., **13** [4] (2022) 610–619.
13. A.S. Alzahrani, G. Pintori, V.M. Sglavo, "Conventional and electric field-assisted ion exchange on glass-ceramics for dental applications", *J. Eur. Ceram. Soc*., **41** [10] (2021) 5341–5348.
14. E.M. Hamzawy, E.A. El-Meliegy, "Preparation of nepheline glass-ceramics for dental applications", *Mater. Chem. Phys*., **112** [2] (2008) 432–435.
15. T.G. Sahama, K. Hytönen, "Götzenite and combeite, two new silicates from the Belgian Congo", *Mineral. Magaz*., **31** [238] (1957) 503–510.
16. Z. Meng, X.S. Yao, H. Yao, Y. Liang, T. Liu, Y. Li, S. Lan, "Measurement of the refractive index of human teeth by optical coherence tomography", *J. Biomed. Optics*, **14** [3] (2009) 034010.
17. K.T. Tait, E. Sokolova, F.C. Hawthorne, A.P. Khomyakov, "The crystal chemistry of nepheline", *Canad. Mineral*., **41** [1] (2003) 61–70.
18. R.A. Martin, S. Yue, J.V. Hanna, P.D. Lee, R.J. Newport, M.E. Smith, J.R. Jones, "Characterizing hierarchical structures of bioactive silicate glass", *Philosoph. Trans. Royal Soc. A*, **370** (2012) 1422–1443.
19. S. Vyazovkin, N. Sbirrazzuoli, "Nonisothermal crystallization kinetics by DSC: Practical overview", *Processes*, **11** [5] (2023) 1438.
20. E.D. Zanotto, "Isothermal and adiabatic nucleation in glass", *J. Non-Crystal. Solids*, **89** [3] (1987) 361–370.
21. A. Deshkar, J. Marcial, S.A. Southern, L. Kobera, D.L. Bryce, J.S. McCloy, A. Goel, "Understanding the structural origin of crystalline phase transformations in nepheline-based glass-ceramics", *J. Am. Ceram. Soc.*, **100** [7] (2017) 2859–2878.
22. G.L. Hovis, D.R. Spearing, J.F. Stebbins, J. Roux, A. Clare, "X-ray diffraction and NMR investigation of nepheline-kalsilite crystalline solutions", *Am. Mineral.*, **77** [1-2] (1992) 19–29.
23. E. Lippmaa, A. Samoson, M. Magi, "High-resolution aluminum-27 NMR of aluminosilicates", *J. Am. Chem. Soc*., **108** [8] (1986) 1730–1735.
24. P. Duxson, G.C. Lukey, F. Separovic, J.S.J. Van Deventer, "Effect of alkali cations on aluminum incorporation in geopolymeric gels", *Indust. Eng. Chem. Res*., **44** [4] (2005) 832–839.
25. X. Xue, J.F. Stebbins, "^{23}Na NMR chemical shifts and local Na coordination environments", *Phys. Chem. Miner*., **20** [5)] (1993) 297–307.
26. A.S. Alzahrani, "Method of forming glass-ceramic materials", *UK Patent No. GB2573650*, 2021.
27. J. McCloy, N. Washton, P. Gassman, J. Marcial, J. Weaver, R. Kukkadapu, "Nepheline crystallization in boron-rich alumino-silicate glasses", *J. Non-Crystal. Solids*, **409** (2015) 149–165.
28. M. Eden, "^{27}Al NMR studies of aluminosilicate glasses", pp. 237–331 in *Annual Reports on NMR Spectroscopy* Vol. 86, Academic Press, 2015.
29. D.R. Neuville, L. Cormier, D. Massiot, "Al coordination in calcium aluminosilicate glasses: Effects of composition determined by ^{27}Al MQ-MAS NMR and Raman spectroscopy", *Chem. Geology*, **229** [1-3] (2006) 173–185.
30. E.M. Hamzawy, E.M. El-Meliegy, "Crystallization in Na_2O-CaO-Al_2O_3-SiO_2-(LiF) glass", *Ceram. Int*., **33** [2] (2007) 227–231.
31. J.F. Stebbins, S. Sen, I. Farnan, "Silicate species exchange and crystallization", *Am. Mineral*., **80** [7-8] (1995) 861–864.
32. V.I. Zakharov, V.A. Matveev, D.V. Mayorov, A.A. Balbukova, T.V. Kondratenko, A.I. Knyazeva, "Effect of nepheline acid processing on silica products", *Russian J. Appl. Chem*., **85** (2012) 1643–1648.
33. H.L. Rittler, "Spontaneously-formed nepheline-carnegieite glass-ceramics", *U.S. Patent No. 4,000,998*. 1977.
34. A.K. Kennedy, T.L. Grove, R.W. Johnson, "Experimental constraints on lava evolution", *Contrib. Mineral. Petrology*, **104** [6] (1990) 722–734.
35. M.I. Martín, F. Andreola, L. Barbieri, F. Bondioli, I. Lancellotti, J.M. Rincón, M. Romero, "Crystallisation and microstructure of nepheline-forsterite glass-ceramics", *Ceram. Int*., **39** [3] (2013) 2955–2966.
36. M. Rampf, M. Dittmer, C. Ritzberger, M. Schweiger, W. Höland, "Properties of $Li_2Si_2O_5$-$Ca_5(PO_4)_3F$ and $Li_2Si_2O_5$-$Sr_5(PO_4)_3F$ glass-ceramics", *Front. Bioeng. Biotechnol*., **3** (2015) 122.